1544–1554 *Nucleic Acids Research, 2013, Vol. 41, No. 3* *Published online 18 December 2012*
doi:10.1093/nar/gks1269

Selective association between nucleosomes with identical DNA sequences

Jun-ichi Nishikawa[1] and Takashi Ohyama[1,2,*]

[1]Department of Biology, Faculty of Education and Integrated Arts and Sciences and [2]Major in Integrative Bioscience and Biomedical Engineering, Graduate School of Science and Engineering, Waseda University, 2-2 Wakamatsu-cho, Shinjuku-ku, Tokyo 162-8480, Japan

Received June 13, 2012; Revised October 30, 2012; Accepted November 5, 2012

ABSTRACT

Self-assembly is the autonomous organization of constituents into higher order structures or assemblages and is a fundamental mechanism in biological systems. There has been an unfounded idea that self-assembly may be used in the sensing and pairing of homologous chromosomes or chromatin, including meiotic chromosome pairing, polytene chromosome formation in *Diptera* and transvection. Recent studies proved that double-stranded DNA molecules have a sequence-sensing property and can self-assemble, which may play a role in the above phenomena. However, to explain these processes in terms of self-assembly, it first must be proved that nucleosomes retain a DNA sequence-sensing property and can self-assemble. Here, using atomic force microscopy (AFM)-based analyses and a quantitative interaction assay, we show that nucleosomes with identical DNA sequences preferentially associate with each other in the presence of Mg^{2+} ions. Using *Xenopus borealis* 5S rDNA nucleosome-positioning sequence and 601 and 603 sequences, homomeric or heteromeric octa- or tetranucleosomes were reconstituted *in vitro* and induced to form weak intracondensates by $MgCl_2$. AFM clearly showed that DNA sequence-based selective association occurs between nucleosomes with identical DNA sequences. Selective association was also detected between mononucleosomes. We propose that nucleosome self-assembly and DNA self-assembly constitute the mechanism underlying sensing and pairing of homologous chromosomes or chromatin.

INTRODUCTION

Self-assembly is the autonomous organization process in which disordered pre-existing components form organized architectures as a consequence of specific, local interactions among the components, without external intervention. Self-assemblies are widely found in physical, chemical and biological processes (1). A characteristic of biological self-assembly is the variety and complexity of the functions of the resulting structures (2,3). For example, self-assembly is used to generate a lipid bilayer, pairing of bases, quaternary structures of proteins, flagella, actin filaments, microtubules, microfibrils, ribosomes and viruses (4–12). Self-assembled structures are thermodynamically more stable than the unassembled components, i.e. the assembled state is generated when a given system can reduce its Gibbs free energy. For example, tobacco mosaic virus, which is composed of RNA and proteins, is decomposed into its components at acidic pH and reformed by growth of a protein polymer on the RNA with rising pH (12). This reformation occurs toward a state of minimum free energy, which is determined by such conditions as the chemical potentials of molecules and ions, temperature and pH (6).

A hierarchy of self-assembling processes is fundamental to cellular function. The complex processes that occur in mitosis and meiosis are likely to involve various self-assembly phenomena (13–15), in which homology sensing or homologous pairing of chromatin or chromosomes is also speculated to be involved. Furthermore, it has long been hypothesized that homologous recombination depends on a self-assembly process between homologous DNA pairs (16–20). With this background, nucleotide sequence-dependent selective interaction between double-stranded (ds) DNA fragments has been studied both theoretically and experimentally. In a theoretical study, it was hypothesized that sequence-dependent twist modulation leads to axial variation of the local helical pitch and this

*To whom correspondence should be addressed. Tel: +81 3 5369 7310; Fax: +81 3 3355 0316; Email: ohyama@waseda.jp

causes an electrostatically favorable alignment of two DNA fragments, in which only DNA with homologous sequences can have negatively charged strands facing positively charged grooves over a large juxtaposition length (21). This hypothesis implies that DNAs with nonhomologous sequences require higher energy for juxtaposition. In another model, it was proposed that non-Watson–Crick hydrogen bond interactions occurring between bases in the major or minor grooves are the basis of homology recognition (16). Local melting could presumably also allow DNA to be juxtaposed (22).

An interesting *in vitro* experiment related to DNA self-assembly reported in 1995 showed that nine single-stranded (ss) GGA repeats that flank a short dsDNA form a parallel-stranded DNA homoduplex in the presence of a near physiological concentration of NaCl (23). This study can be regarded as an example of the assembly of ssDNA molecules with the same sequence. More than a decade later, in 2007, experimental evidence for the sequence-dependent selective assembly of dsDNA molecules was obtained using electrophoretic analysis and atomic force microscopy (AFM) (22). This study showed that DNA molecules in the presence of physiological concentrations of Mg^{2+} ions can distinguish 'self' and 'non-self' and self-assemble even in a solution of heterogeneous DNA species. Even curved DNA can self-assemble, indicating that this phenomenon seems to be general for all kinds of dsDNA. Subsequently, other experimental approaches have confirmed this property of DNA. In one experiment, liquid-crystalline aggregates (spherulites) were prepared using two fluorescently tagged dsDNA fragments with different sequences and spontaneous segregation of the two kinds of dsDNA within each spherulite was observed (24). Another study used a parallel single molecule magnetic tweezers-based assay to show the presence of sequence-directed protein-independent dsDNA/dsDNA pairing (25).

If self-assembly is involved in the pairing of chromatin and chromosomes, it is particularly important to examine whether nucleosomes, the fundamental units of chromatin (26), have sequence-dependent self and non-self discrimination properties, since genetic events in eukaryotes usually occur on chromatin. At present, however, no evidence has been found for homology-sensing and self-assembling properties of nucleosomes. In this study, we show selective association between nucleosomes with identical DNA sequences using AFM and a quantitative interaction assay. This self-assembly of nucleosomes, along with those of dsDNA, can explain the mechanism underlying the intimate pairing of homologs in meiotic chromosome pairing, polytene chromosome formation in *Diptera*, transvection and other similar phenomena (27–30).

MATERIALS AND METHODS

DNA templates

601 and 5S octamers

The 601 sequence (31) and the *Xenopus borealis* 5S rDNA nucleosome-positioning sequence (32) were amplified by polymerase chain reaction (PCR) using the plasmid pGEM3Z-601 (a gift from Dr Widom) and *X. borealis* genomic DNA, respectively. The PCR primers are shown in Supplementary Table S1: primers #1 and #2 for 601 octamer and primers #3 and #4 for 5S octamer. These primers also contained linker DNA sequences. The octamers were generated as follows. Each PCR product was digested with BamHI and BglII to generate a unit fragment (Supplementary Figure S1) and inserted into the BamHI site of pUC19. Subsequently, the unit fragment was again inserted into the BamHI site of the recombinant plasmid. The plasmid carrying a tandem dimer of the unit was then screened. Insertion of the unit fragment and screening were repeated and a plasmid containing octameric repeats of each unit sequence was obtained. Finally, the resulting plasmids were digested with SacI and XbaI, and the 601 and 5S octamers were gel purified.

601/5S chimera

Using the stepwise procedure described above, plasmids containing tetrameric repeats of the 601 sequence and the 5S rDNA nucleosome-positioning sequence were obtained. The former plasmid was digested with BamHI and SalI to give a tetrameric repeat of the 601 sequence. This fragment was inserted between BamHI and SalI site of the latter plasmid. Finally, the resulting plasmid was digested with SacI and XbaI and the 601/5S chimera was gel purified.

601 and 603 tetramers

The 603 sequence (31) was amplified by PCR from pGEM3Z-603 (a gift from Dr Widom). The PCR primer sets are shown in Supplementary Table S1: primers #5 and #6 for the 601 sequence with a 30-bp linker DNA; primers #7 and #8 for the 603 sequence with a 30-bp linker DNA; primers #9 and #10 for the 601 sequence with a 62-bp linker DNA and primers #11 and #12 for the 603 sequence with a 62-bp linker DNA. The PCR fragments were digested with BanII and gel purified to generate the unit fragments (Supplementary Figure S1). Ligation of BanII fragments generates head-to-tail binding because of the lack of rotational symmetry in the 5′-GGGCTC-3′ site. Partial ligation of each BanII fragment generated the 601 and 603 tetramers. These were cloned into the BanII site of the plasmid pUC19asBanII, which was constructed by inserting the sequence 5′-AATTCGGGCTCGGATC-3′ ('asBanII' adapter) between the EcoRI and BamHI sites of pUC19, recovered from the recombinants by digestion with EcoRI and BamHI and finally gel purified.

AABB and ABAB chimeras

Equal amounts of the 601 and 603 unit fragments (BanII fragments) described above were mixed and partial ligation was performed. The fragments of the tetramer size were recovered from 1.0% agarose gel, inserted into pUC19asBanII and cloned. Plasmids containing the AABB or ABAB chimera were screened and these chimeras were recovered from the recombinant plasmids with EcoRI and BamHI digestion and gel purified. All constructs were sequenced for verification.

Biotinylated or Alexa 555-labeled 601 and 603 fragments

The 601 and 603 sequences were amplified by PCR from pGEM3Z-601 and pGEM3Z-603, respectively, using the primer sets shown in Supplementary Table S1: primers #13 and #14 for the biotinylated 601 fragment; primers #15 and #16 for the biotinylated 603 fragment; primers #17 and #18 for the Alexa 555-labeled 601 fragment and primers #19 and #20 for the Alexa 555-labeled 603 fragment. Preparation of Alexa 555-labeled DNA fragments was performed according to Baldwin *et al.* (24). All the DNA fragments were gel purified. Fluorescence intensities of the fragments were measured as band intensities on agarose gels using the Typhoon-9410 (Amersham Biosciences) and ImageQuant software (Molecular Dynamics). Specific activities of the labeled fragments were adjusted to be the same for the 601 and 603 fragments using unlabeled fragments.

In vitro nucleosome reconstitution

Histone cores were purified from chicken erythrocytes (Nippon Bio-Test Laboratories) according to Thorne *et al.* (33). Nucleosomes were reconstituted *in vitro* by the double-dialysis method (34). The reconstitution solution of 50 µl contained 1 µg (for reconstitution of octa- and tetranucleosomes) or 0.5 µg (for mononucleosomes) of DNA templates, 0.63–0.96 µg (for reconstitution of octa- and tetranucleosomes) or 0.40–0.46 µg (for mononucleosomes) of histone cores, 10 mM Tris–HCl (pH 7.5), 0.7 mM β-mercaptoethanol and 2.0 M NaCl. This solution was then dialyzed against a buffer comprising 10 mM Tris–HCl (pH 7.5) and 0.7 mM β-mercaptethanol. In the quantitative assay of mononucleosome–mononucleosome association, solutions of Alexa 555-labeled nucleosome were concentrated 5-fold using Amicon filters (Millipore). Nucleosome formation was confirmed electrophoretically using 2% polyacrylamide/1% agarose composite gels (for octa- and tetranucleosomes; Supplementary Figures S2A and S3A and B) or 4% native polyacrylamide gels (for mononucleosomes).

AFM analyses

Appropriate amounts of $MgCl_2$ solutions were added to nucleosome solutions to prepare the Mg^{2+} concentrations indicated in the figures. The resulting solutions were incubated for 5 min. Then, glutaraldehyde was added to each solution to a level of 0.1% and the mixture was incubated for 5 min. This condition was the most appropriate and effective, among the conditions examined (Supplementary Figure S4). Freshly cleaved mica was pre-coated with 50 µl of 10 µg/ml poly-L-lysine (PL) (Sigma) for 3 min and dried. Nucleosome solutions (40 µl) were deposited onto the PL-coated micas. After 3 min, these were rinsed three times with 100 µl of Milli-Q water and gently dried. AFM images were obtained with the Nanowizard II (JPK Instruments) operating in intermittent contact mode (air) using OMCL-AC160TS-W2 (Olympus) and SSS-NCH (Nanosensors) silicon probes. Scan rates were 1.6 Hz. More than 12 different fields on a slide were randomly selected and subjected to analysis. Images were processed using JPK Image Processing software (JPK Instruments). The population analysis for the intracondensates of octanucleosomes was performed as follows. The intracondensates were sorted into seven types by visual inspection at first. Subsequently, the volume ratios between the globules in an intracondensate were scrutinized for each of the 2565 image samples by using the Gwyddion software (http://www.gwyddion.net/) and only defined samples (2469 images) were left for the population calculation.

Quantitative association assay

Nucleosomes were first fixed on magnetic beads in a 20 µl solution containing 50 µg Dynabeads M-280 streptavidin (Invitrogen/Dynal), 930 ng biotinylated nucleosomes and TGN buffer [10 mM Tris–HCl (pH 7.5), 5% glycerol and 0.01% NP-40]. The mixture was incubated on a rotator at 4°C for 1.5 h. The beads carrying nucleosomes were washed twice with 500 µl of TGN buffer at 4°C for 5 min and resuspended in 80 µl of TGN buffer. Then, 1 µl of Alexa 555-labeled nucleosomes and 5 µl of TGN buffer containing 0, 1.0, 2.0 or 3.0 mM $MgCl_2$ were added to 4 µl of the suspension of beads described above. After incubation of the resulting suspension on a shaker at 25°C for 5 min, 10 µl of a solution containing 0.5% glutaraldehyde, TGN buffer and 0, 0.5, 1.0 or 1.5 mM $MgCl_2$ was added. After an additional 10-min incubation under the same conditions, the reaction was quenched by adding 1 µl of 2.5 M glycine and further incubated for 5 min. The magnetic beads carrying associated nucleosomes were then washed with 500 µl of TGN buffer three times. The beads were then mixed with other beads bearing both Alexa 555-labeled 5′-AAAAAA-3′ (A_6) and Alexa 647-labeled A_6 in 10 µl of TGN buffer. The latter beads were prepared according to the manufacturer's recommendations and were used as an internal intensity standard. The beads mixture was deposited onto a slide, and images were captured with an Olympus Fluoview FV1000-D confocal microscope equipped with a 60× oil-immersion lens. The fluorescence intensity on the magnetic beads was measured using NIH ImageJ as follows. The contour of each bead was encircled and its gross fluorescence intensity (*a*) was measured; a circle with the same diameter was placed near the bead and its gross intensity (*b*, background) was measured. The fluorescence intensity generated by the association of Alexa-labeled nucleosomes was calculated as *a*–*b*. In each experiment, eight different fields on a slide were randomly selected and fluorescence intensities of all beads (~60 on average) were analyzed and averaged. Calibration of the intensities of the fluorescence between different observations was performed by using the fluorescence intensities of the internal control beads described above. To obtain each data point, independent experiments were performed seven times.

Statistics

All results are presented as a mean ± SD or SEM, as indicated. *P*-values were calculated using an unpaired Student's *t*-test (two-tailed).

RESULTS

AFM-based analyses suggest a phenomenon of DNA sequence-based selective association between nucleosomes

We first reconstituted octanucleosomes *in vitro* (Supplementary Figure S2A), induced condensation of the component nucleosomes (Supplementary Figure S2B) and investigated the structure of the condensates. The octanucleosomes were prepared using histone cores from chicken erythrocytes and the following DNA templates: an eight-time repeat of the 601 sequence (31) (referred to as the '601 octamer' below), an eight-time repeat of *X. borealis* 5S rDNA nucleosome-positioning sequence (32) (5S octamer) and a chimera of a four-time repeat of the 601 sequence and a four-time repeat of the 5S rDNA (601/5S chimera) (Figure 1A). The resulting octanucleosomes were named as the 'octa-601 array', 'octa-5S array' and 'chimeric array', respectively. Nucleosome condensation was induced by $MgCl_2$. Since glutaraldehyde can fix cation-induced condensates of nucleosomes (35), we treated the nucleosome condensates with the reagent very weakly ('Materials and Methods' section and Supplementary Figure S4). Then, the shapes of 'intracondensates' were analyzed by AFM. Theoretically, intracondensates can be categorized into seven types according to the number of 'globules'. Here, the types are indicated with a number, as shown in Figure 1B. Regarding the profile of the condensate types (Figure 1C) at 0.25 or 1.0 mM Mg^{2+}, the chimeric array was similar to the octa-601 array at 0.25 mM and to the octa-5S array at 1.0 mM, but clearly dissimilar to these homomeric arrays at 0.5 mM Mg^{2+}. At this concentration, the homomeric arrays had almost the same profiles. With an increase in Mg^{2+} ions, the 1g type increased in all arrays, as expected.

If DNA-based selective association occurs between nucleosomes, the chimeric array will, compared with the homomeric arrays, generate a higher amount of dumbbell-shaped condensates, which are categorized into type 2g in Figure 1B. Thus, we focused on this type. At 0.5 mM Mg^{2+}, the chimeric array generated the 2g type much more abundantly than the homomeric arrays (Figure 1C, yellow line). Theoretically, the 2g-type condensates can be further classified into four forms: 7-1 (numerals indicate the number of nucleosomes involved in a globule), 6-2, 5-3 and 4-4 (dumbbell-shaped) forms. Indeed, as shown in Figure 1D, all forms were detected in particle-size analysis ('Materials and Methods' section). Interestingly, among these four forms of the chimeric array, form 4-4 was the most abundant at 0.5 mM Mg^{2+} (Figure 1E, left panel). Furthermore, with this array, form 4-4 was also the most common form at 0.25 and 1.0 mM. On the other hand, the octa-601 and octa-5S arrays hardly generated this form, but instead favored the 6-2 form (and the 5-3 form for the octa-5S array) at all Mg^{2+} concentrations examined (Figure 1E, center and right panels). Thus, these analyses strongly suggest a phenomenon of DNA sequence-based selective association between nucleosomes. However, this association may be weak, and topological stresses may prevent it in some cases. This hypothesis can explain why the homomeric arrays did not generate more 1g-type condensates than the chimeric arrays, i.e. the most abundant 6-2 or 5-3 form in the 2g-type condensates of homomeric arrays may generate the 1g-type condensates accompanied with some topological stress, while the most abundant 4-4 form in the 2g-type condensates of heteromeric arrays can generate the 1g-type condensates without any topological stress. In the latter case, presumably, the topological merit could overcome the obstacles originating from the unfavorable interactions between different kinds of nucleosomes. Regardless of the hypothesis, the ability of this analysis to yield a conclusion is somewhat limited, because of the complexity of the folded structures of the octanucleosomes and the resolution of the AFM.

Nucleosomes can sense homology and self-assemble

We then performed a similar, but more accurate, analysis using four-time repeats of the 601 sequence (601 tetramer) and 603 sequence (603 tetramer), and two composite sequences comprising the 601 and 603 sequences, referred to as the 'AABB chimera' and 'ABAB chimera' (Figure 2A). The 603 sequence is an artificially constructed DNA with high affinity for histone cores (31). The resulting tetranucleosomes (Supplementary Figure S3A and B) are named as shown in Figure 2A. These allowed us to distinguish the paths of the three linker DNAs. The intracondensates are categorized into three types in this case (Figure 2B). Except for the tetra-603 array with 30 bp linkers, in which condensation proceeded slightly more than for the other arrays, the 3g type was the most abundant in the condensates of each array at all Mg^{2+} concentrations examined (Figure 2C). However, this difference did not influence the analysis. In this experiment, we focused on the 3g type, in which two nucleosomes are associated and the other two are free. This type, classified into four forms (Figure 2D), is thought to be generated just at the start of condensation.

We analyzed the population ratio (%) of each form in the entire population of the 3g type (Figure 2E and F and Supplementary Figure S3C and D). At first, the analysis was performed using nucleosome arrays with a linker length of 30 bp (Figure 2E). We cannot distinguish the 5′- and 3′-ends of the arrays in the current procedure. Thus, the nucleosomes 1-and-2- and 3-and-4-associated arrays (form I) cannot be distinguished from each other, and similarly the 1-and-3- and 2-and-4-associated arrays (form IV) cannot be distinguished from each other (see schematic depiction in Figure 2D). Thus, if the interaction is equivalent among the four nucleosomes in an array, the counted population of form I or IV will be 2-fold that of form II or III and the theoretical percentages of each form in the 3g type will be I, 33.3%; II, 16.7%; III, 16.7% and IV, 33.3%. With reference to these values, Figure 2E suggests that the interaction was generally not equivalent among the four nucleosomes in each array. However, the extent of the deviation from the percentages above was relatively small for the tetra-601 and tetra-603 (homomeric) arrays. On the other hand, some forms of the AABB and ABAB (heteromeric) arrays showed

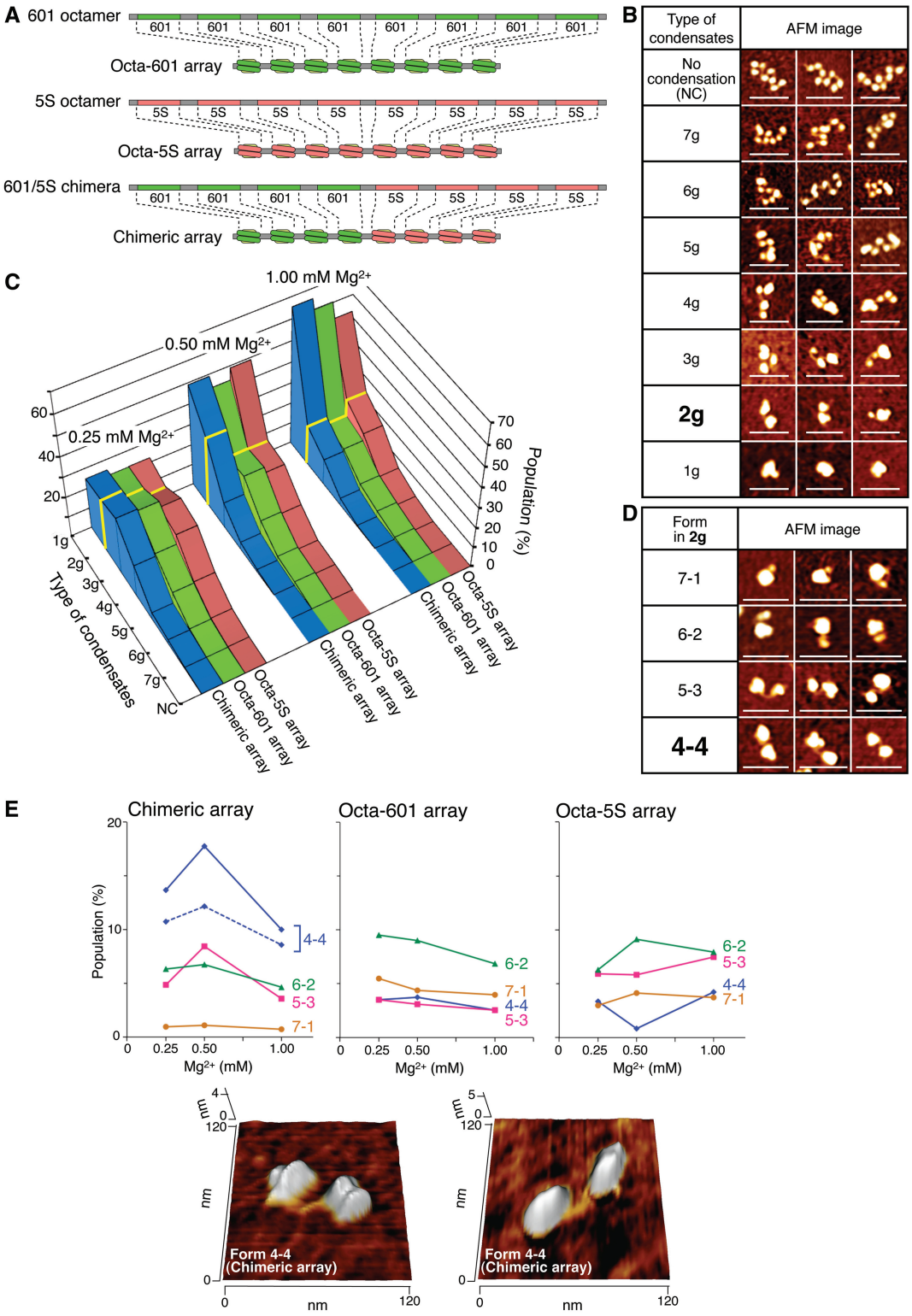

Figure 1. Magnesium ion-induced condensation of octanucleosomes reconstituted *in vitro*. (**A**) DNA templates used in the reconstitution and the resulting nucleosomal arrays (also see Supplementary Figure S1). (**B**) Types of intracondensates and representative AFM images. The types are indicated by the number of globules. A nucleosome and a condensate of nucleosomes are each counted as a single globule. Bars indicate 100 nm. (**C**) Population ratio of each type of condensate relative to the entire population of octanucleosomes at 0.25, 0.50 or 1.0 mM Mg^{2+}. The population ratio of the 2g type is indicated with a yellow line. 'NC' indicates octanucleosomes with no condensation; $n \geq 205$ for each array. (**D**) Four forms of condensate type 2g. Bars indicate 100 nm. (**E**) Population ratio of each form of 2g relative to the entire population of octanucleosomes at 0.25, 0.50 or 1.0 mM Mg^{2+}. For the 4-4 form of the chimeric array, two data sets are shown. The lower set (dotted line) indicates the data points for the 4-4 form with purely separated nucleosome species, as judged from the number of bridge lines (linker DNA) between the globules: a single bridge line means that each globule is comprised of a single nucleosome species. The upper set (solid line) indicates the data points for all the 4-4 forms. 4-4 forms with unclear linker image are included in calculating the upper data set. Representative AFM images of form 4-4 of the chimeric array are also shown.

surprising deviations. The biggest deviations were observed for productions of form I of the AABB array and form IV of the ABAB array. These are products of nucleosome 'self-association' (meaning association between the same nucleosome species). Very interestingly, these accounted for >55% in most Mg^{2+} conditions. Furthermore, all the forms generated by 'non-self-association' were clearly disfavored in these heteromeric arrays. As shown in Figure 2F, when the linker length was extended to 62 bp, the population balances among the 3g forms changed slightly from those in Figure 2E. However, self-associations were clearly favored and non-self-associations were generally disfavored in the heteromeric arrays. Thus, the phenomenon of self-association was found not to depend on the linker length. The fixative was used to obtain stable (incapable of being disassembled) samples to facilitate manipulations. However, even in the absence of the reagent, we obtained essentially the same results (Supplementary Figure S5).

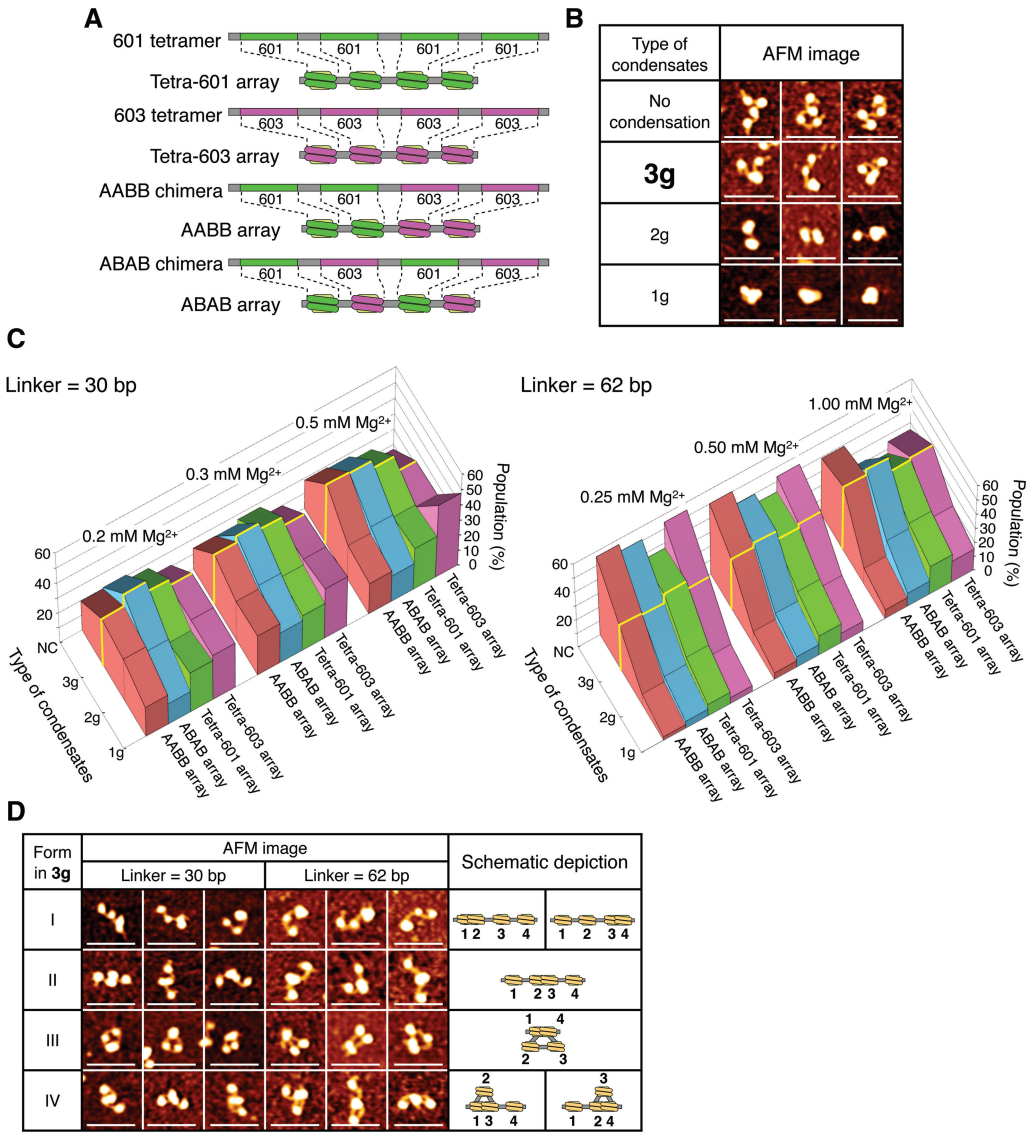

Figure 2. Discrimination of association between nucleosomes in chimeric tetranucleosomal arrays. (**A**) DNA templates and nucleosomal arrays (see also Supplementary Figure S1). (**B**) Types of intracondensates and representative AFM images. The types are indicated by the number of globules, as in Figure 1. Bars indicate 100 nm. (**C**) Population ratio of each type of condensate relative to the entire population of tetranucleosomes at the indicated concentrations of Mg^{2+}. The population ratio of the 3g type is indicated with a yellow line. 'NC' indicates tetranucleosomes with no condensation. The population ratios are mean values of three independent determinations. Across the range of Mg^{2+} concentrations, the total count of tetranucleosomes ranged from 88 to 508 (usually ~200). (**D**) Four forms of type 3g. Bars indicate 100 nm. (**E** and **F**) Population ratio of each form of condensate relative to the entire population of the 3g-type condensates at the indicated concentrations of Mg^{2+}. The linker DNA lengths were 30 bp (E) and 62 bp (F). The light blue and brown dotted lines indicate 16.7 and 33.3%, respectively (see text). The condensates were generated three times as described above, using at least two independently reconstituted samples. Data are shown as means ± SD ($n = 3$). For form I of the AABB array and form IV of the ABAB array, the *P*-values for comparison of the corresponding data for the tetra-601 array (upper) and tetra-603 array (lower) are indicated. $*P < 0.05$; $**P < 0.01$. Representative AFM images of form I of the AABB array and form IV of the ABAB array are also shown.

(continued)

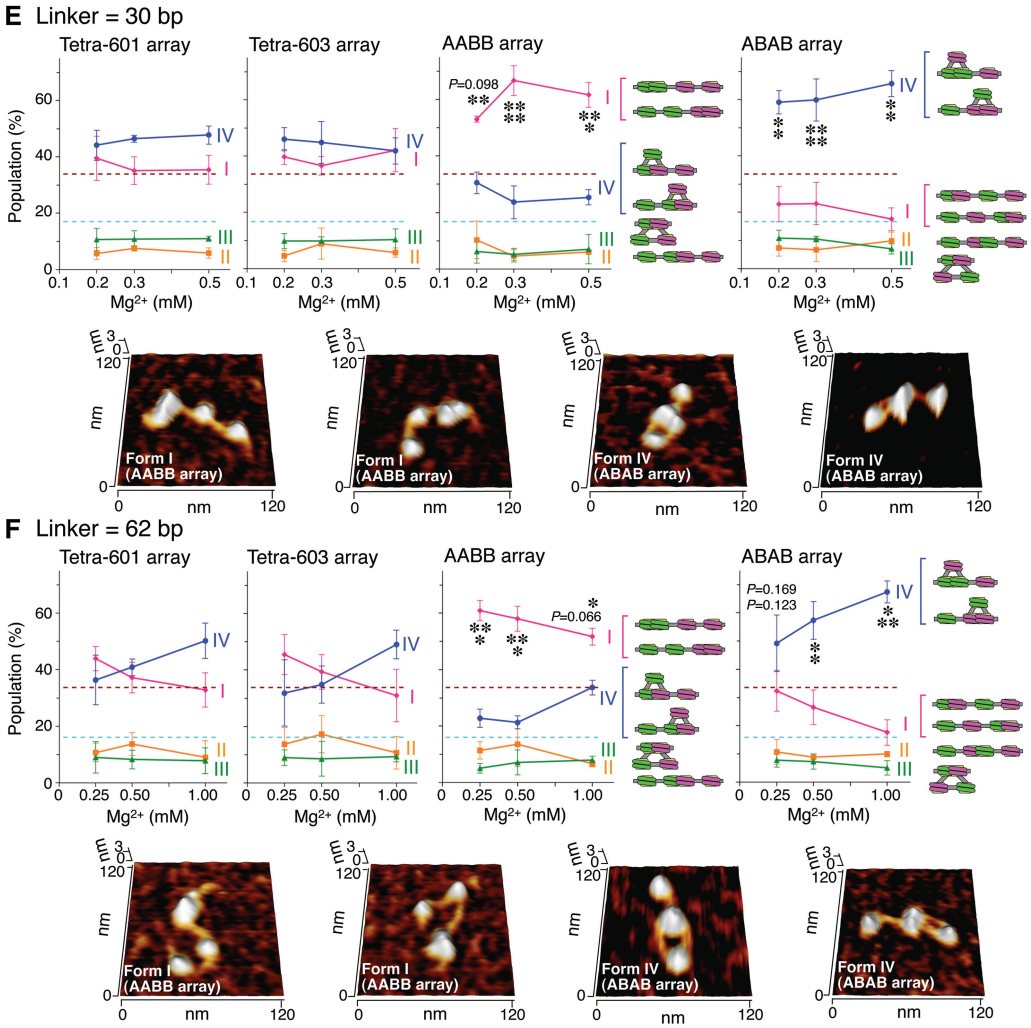

Figure 2. Continued.

DNA sequence-based selective association between nucleosomes is confirmed by a quantitative interaction assay

In the experiments described above, movements of nucleosomes were restricted by linker DNAs. In the final set of experiments, nucleosome–nucleosome interaction was examined in a system free from such restriction. Association between bead-fixed mononucleosomes and Alexa 555-labeled mononucleosomes was monitored as the increase in fluorescence intensity on the beads (Figure 3A). As shown in Figure 3B, this assay clearly showed that associations between the same nucleosome species were preferred over those between different species.

DISCUSSION

AFM-based analyses using homomeric or heteromeric octa- or tetranucleosomes and a quantitative interaction assay using mononucleosomes showed that nucleosomes with identical DNA sequences preferentially associate with each other in the presence of physiological concentrations of Mg^{2+} ions. This finding, along with recent findings of sequence-dependent dsDNA self-assembly (22,24,25), provides a tangible clue to the mechanism underlying homologous pairing of chromatin or chromosomes, which is widely observed in eukaryotes.

A putative mechanism underlying nucleosome self-assembly

As shown in this study, nucleosomes can distinguish self from non-self based on the nucleotide sequence of DNA wrapped around the histone core. This conclusion is reinforced in this study by the use of '*in vivo* histones' that were heterogeneously modified, but with which self-assembly phenomena were clearly detected. These results raise the question of which properties of DNA cause this phenomenon. DNA sequence-based selective association of nucleosomes occurs in the presence of Mg^{2+}. Thus, the requirement of Mg^{2+} ions is an important hint in understanding the mechanism. Mg^{2+} ions can also induce or stabilize self-assembly of naked dsDNA fragments (22), and monovalent cations have also been

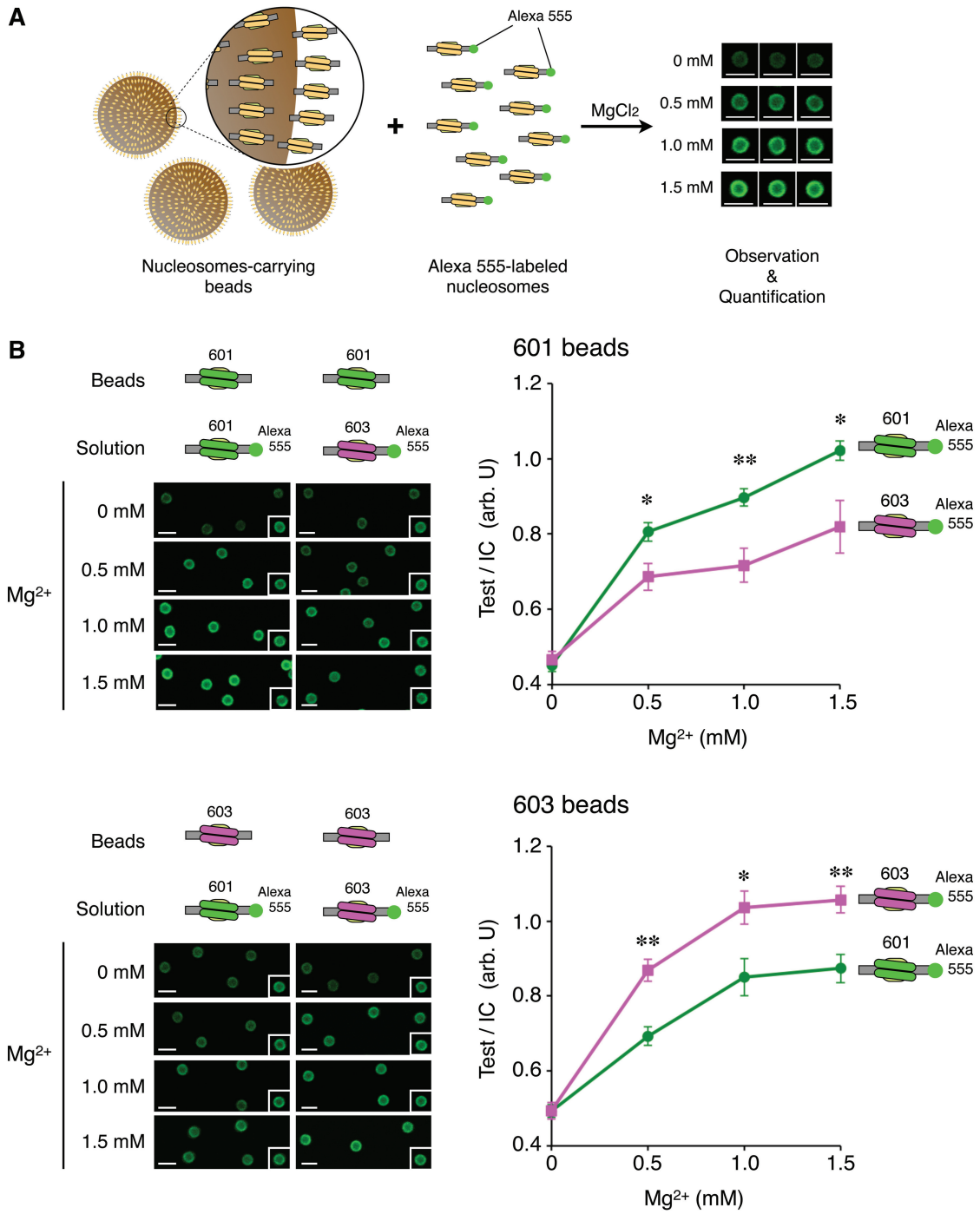

Figure 3. DNA-sequence-based preferential association between nucleosomes. (**A**) An assay for quantifying association between nucleosomes. Magnetic beads carrying nucleosomes were mixed with Alexa 555-labeled nucleosomes in the presence or absence of Mg^{2+}. The associated nucleosomes were fixed and quantified using fluorescence microscopy. Bars indicate 5 μm. (**B**) Microscopic images (left) and quantification (right) of the association of Alexa 555-labeled nucleosomes with magnetic beads carrying nucleosomes. The fluorescence intensity generated by the association of Alexa 555-labeled nucleosomes (test) was calibrated by using the intensity of the internal control (IC). For beads used for the IC, see 'Materials and Methods' section. They were distinguished from test samples by detecting fluorescence of Alexa 647. The inset in each panel shows the IC bead. Mg^{2+}-induced increase in fluorescence intensity on the beads is shown as a function of Mg^{2+} concentration. The focus was adjusted on the plane involving the 'equator line' of each bead. Bars indicate 5 μm. Data are shown as means ± SEM ($n = 7$). $*P < 0.05$; $**P < 0.01$.

reported to help self-assembly of naked dsDNA (25). Considering that free dsDNA and nucleosomal DNA have different topologies (linear versus supercoiled), it seems that the mechanism underlying the DNA self-assembly and that underlying the nucleosome self-assembly are different, but the mechanisms have Mg^{2+} ions in common. These ions coordinate with phosphate oxygen atoms and the N7 and O6 atoms of

guanosine (36,37) and can stabilize the DNA duplex by alleviating electrostatic repulsive interactions between phosphates in the sugar-phosphate backbone (38). Thus, reduction of electrostatic repulsion may also be the principal role of Mg^{2+} ions in nucleosome self-assembly. These conditions of low or no electrostatic repulsion may allow nucleosomes to interact with each other in a nucleotide sequence-dependent manner. Here, we note that Ca^{2+} ions also exerted very similar effects under the conditions examined (Supplementary Figure S6), although the experiment was not systematic, when compared with Figure 2.

When the condensation of homologous nucleosomes is compared with that of heterologous nucleosomes, the former may be thermodynamically favored, for an unknown reason. The most plausible conformations of the form I condensates and those of the form IV condensates of tetranucleosomal arrays (Figure 2D) are shown in Figure 4A (of the four nucleosomes, three are extracted and their topologies are shown). A somewhat similar arrangement is seen in the crystal packing of nucleosomes and in some models (39–43). The major contact sites in these condensates lie between the core histones, rather than the DNA surfaces. This arrangement of nucleosomes may reduce the free energy of the system. However, at present, we cannot explain how the DNA homology is involved in this putative thermodynamic benefit. Regardless, we may reasonably conclude that the mechanisms underlying the self-assembly of homologous dsDNAs and those underlying the self-assembly of homologous nucleosomes are different.

Nucleosome self-assembly and homologous pairing of chromosomes

The mechanism underlying the self-recognition and pairing of two homologous chromosomes in the early prophase of meiosis I is a major mystery in cell biology (20,44). The same is true for 'somatic pairing' such as polytene chromosome formation observed in *Diptera* (29) and in transvection (30,45). Polytene chromosomes are generated when multiple rounds of replication produce many sister chromatids that remain together. Transvection is a phenomenon that usually occurs through an interaction between an allele on one chromosome and the corresponding allele on the homologous chromosome and can activate or repress genes epigenetically. Many other phenomena also involve homologous pairing of chromatin (30), but the mechanism

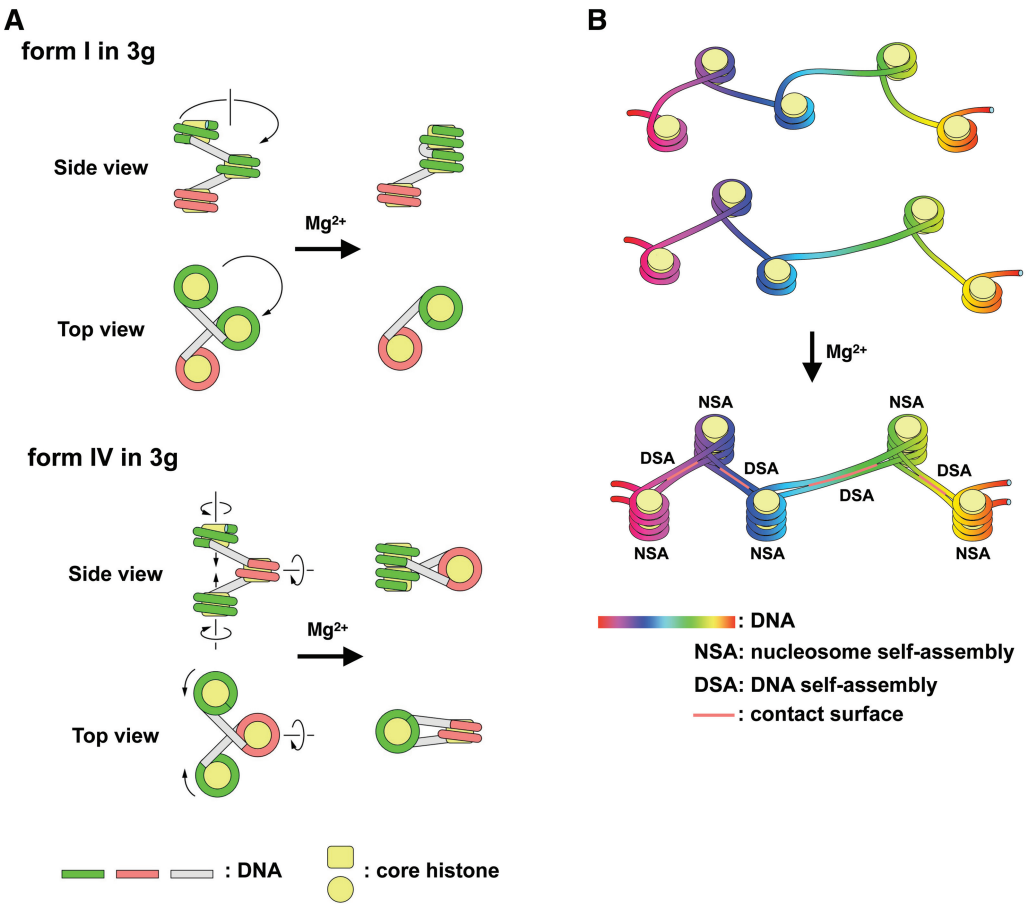

Figure 4. Topology of nucleosome self-assembly and its hypothetical figure in the pairing of homologous chromatin. (**A**) Possible topologies of associated nucleosomes in the form I and form IV condensates of tetranucleosomal arrays. For 3g, form I and form IV, see Figure 2. Only three nucleosomes in the form I and form IV condensates are extracted. DNAs with the same sequence have the same color. (**B**) A hypothetical schema depicting nucleosome–nucleosome and DNA–DNA associations in the pairing of homologous chromatin.

through which homologs uniquely pair with each other is poorly understood. In some cases, specific chromosome locus seems to be involved at the first step of pairing (46). A very recent report for fission yeast showed that noncoding RNA mediates this step (47). Furthermore, the RNAi components have been suggested to contribute to the stabilization of chromosomal pairing between Polycomb group response elements (48). However, they seem to be dispensable, at least in meiotic and early somatic pairing in *Drosophila* (49). Furthermore, in somatic homolog pairing in *Drosophila*, there seems to be no required zygotic gene product (50). Besides the above-mentioned noncoding RNA in fission yeast (47), long-distance interactions and rough apposition (alignment) between dispersed homologous chromosomes may be mediated by the binding of various chromatin-bound proteins including transcriptional machinery proteins, cohesin, insulator and Polycomb proteins (49,51,52). However, the mechanism underlying the intimate association of homologs is still unclear.

Finally, we hypothesize that the nucleosome self-assembly shown in this study and DNA self-assembly (22,24,25) are essential mechanisms in the intimate association of homologs (Figure 4B). Nucleosome self-assembly may also be used in folding of repetitive DNA sequences into ordered chromatin, such as in formation of centromeric chromatin (14,53). A further important issue to be explored is the effect of DNA methylation on nucleosome self-assembly and DNA self-assembly, and this work is now in progress.

SUPPLEMENTARY DATA

Supplementary Data are available at NAR Online: Supplementary Table 1 and Supplementary Figures 1–6.

ACKNOWLEDGEMENTS

The authors thank J. Widom for pGEM3Z-601 and pGEM3Z-603 plasmids. We thank T. Kohwi-Shigematsu for valuable discussion and S. Asano for technical assistance.

FUNDING

Grants-in-Aid from the Ministry of Education, Culture, Sports, Science & Technology—Japan (MEXT) (to T.O.). Funding for open access charge: Grants-in-Aid from MEXT.

Conflict of interest statement. None declared.

REFERENCES

1. Whitesides,G.M. and Grzybowski,B. (2002) Self-assembly at all scales. *Science*, **295**, 2418–2421.
2. Kushner,D.J. (1969) Self-assembly of biological structures. *Bacteriol. Rev.*, **33**, 302–345.
3. Perham,R.N. (1975) Self-assembly of biological macromolecules. *Philos. Trans. R. Soc. Lond. B*, **272**, 123–136.
4. Mueller,P., Rudin,D.O., Tien,H.T. and Wescott,W.C. (1962) Reconstitution of cell membrane structure *in vitro* and its transformation into an excitable system. *Nature*, **194**, 979–980.
5. Watson,J.D. and Crick,F.H.C. (1953) Molecular structure of nucleic acids: a structure for deoxyribose nucleic acid. *Nature*, **171**, 737–738.
6. Oosawa,F. and Asakura,S. (1975) *Thermodynamics of the Polymerization of Protein*. Academic Press, London.
7. Asakura,S. (1968) A kinetic study of *in vitro* polymerization of flagellin. *J. Mol. Biol.*, **35**, 237–239.
8. Horváth,I., Király,C. and Szerb,J. (1949) Action of cardiac glycosides on the polymerization of actin. *Nature*, **164**, 792.
9. Miki-Noumura,T. and Mori,H. (1972) Polymerization of tubulin: the linear polymer and its side-by-side aggregates. *J. Mechanochem. Cell Motil.*, **1**, 175–188.
10. Fraser,R.D., MacRae,T.P. and Suzuki,E. (1976) Structure of the alpha-keratin microfibril. *J. Mol. Biol.*, **108**, 435–452.
11. Traub,P. and Nomura,M. (1969) Structure and function of *Escherichia coli* ribosomes. VI. Mechanism of assembly of 30 s ribosomes studied *in vitro*. *J. Mol. Biol.*, **40**, 391–413.
12. Fraenkel-Conrat,H. and Williams,R.C. (1955) Reconstitution of active tobacco mosaic virus from its inactive protein and nucleic acid components. *Proc. Natl Acad. Sci. USA*, **41**, 690–698.
13. Öllinger,R., Alsheimer,M. and Benavente,R. (2005) Mammalian protein SCP1 forms synaptonemal complex-like structures in the absence of meiotic chromosomes. *Mol. Biol. Cell*, **16**, 212–217.
14. Carroll,C.W. and Straight,A.F. (2006) Centromere formation: from epigenetics to self-assembly. *Trends Cell Biol.*, **16**, 70–78.
15. Mogilner,A. and Craig,E. (2010) Towards a quantitative understanding of mitotic spindle assembly and mechanics. *J. Cell Sci.*, **123**, 3435–3445.
16. McGavin,S. (1971) Models of specifically paired like (homologous) nucleic acid structures. *J. Mol. Biol.*, **55**, 293–298.
17. Wilson,J.H. (1979) Nick-free formation of reciprocal heteroduplexes: a simple solution to the topological problem. *Proc. Natl Acad. Sci. USA*, **76**, 3641–3645.
18. McGavin,S. (1989) Four strand recombination models. *J. Theor. Biol.*, **136**, 135–150.
19. Rocco,V. and Nicolas,A. (1996) Sensing of DNA non-homology lowers the initiation of meiotic recombination in yeast. *Genes Cells*, **1**, 645–661.
20. Cherstvy,A.G. (2011) DNA–DNA sequence homology recognition: physical mechanisms and open questions. *J. Mol. Recognit.*, **24**, 283–287.
21. Kornyshev,A.A. and Leikin,S. (2001) Sequence recognition in the pairing of DNA duplexes. *Phys. Rev. Lett.*, **86**, 3666–3669.
22. Inoue,S., Sugiyama,S., Travers,A.A. and Ohyama,T. (2007) Self-assembly of double-stranded DNA molecules at nanomolar concentrations. *Biochemistry*, **46**, 164–171.
23. Suda,T., Mishima,Y., Asakura,H. and Kominami,R. (1995) Formation of a parallel-stranded DNA homoduplex by d(GGA) repeat oligonucleotides. *Nucleic Acids Res.*, **23**, 3771–3777.
24. Baldwin,G.S., Brooks,N.J., Robson,R.E., Wynveen,A., Goldar,A., Leikin,S., Seddon,J.M. and Kornyshev,A.A. (2008) DNA double helices recognize mutual sequence homology in a protein free environment. *J. Phys. Chem. B*, **112**, 1060–1064.
25. Danilowicz,C., Lee,C.H., Kim,K., Hatch,K., Coljee,V.W., Kleckner,N. and Prentiss,M. (2009) Single molecule detection of direct, homologous, DNA/DNA pairing. *Proc. Natl Acad. Sci. USA*, **106**, 19824–19829.
26. Luger,K., Mäder,A.W., Richmond,R.K., Sargent,D.F. and Richmond,T.J. (1997) Crystal structure of the nucleosome core particle at 2.8 Å resolution. *Nature*, **389**, 251–260.
27. Weiner,B.M. and Kleckner,N. (1994) Chromosome pairing via multiple interstitial interactions before and during meiosis in yeast. *Cell*, **77**, 977–991.
28. Gerton,J.L. and Hawley,R.S. (2005) Homologous chromosome interactions in meiosis: diversity amidst conservation. *Nat. Rev. Genet.*, **6**, 477–487.
29. Riede,I. and Renz,M. (1983) Study on the somatic pairing of polytene chromosomes. *Chromosoma*, **88**, 116–123.
30. Wu,C.T. and Morris,J.R. (1999) Transvection and other homology effects. *Curr. Opin. Genet. Dev.*, **9**, 237–246.
31. Lowary,P.T. and Widom,J. (1998) New DNA sequence rules for high affinity binding to histone octamer and sequence-directed nucleosome positioning. *J. Mol. Biol.*, **276**, 19–42.

32. Hayes,J.J. and Wolffe,A.P. (1993) Preferential and asymmetric interaction of linker histones with 5S DNA in the nucleosome. *Proc. Natl Acad. Sci. USA*, **90**, 6415–6419.
33. Thorne,A.W., Cary,P.D. and Crane-Robinson,C. (1998) Extraction and separation of core histones and non-histone chromosomal proteins. In: Gould,H. (ed.), *Chromatin: A Practical Approach*. Oxford University Press, New York, pp. 35–57.
34. Thåström,A., Lowary,P.T. and Widom,J. (2004) Measurement of histone–DNA interaction free energy in nucleosomes. *Methods*, **33**, 33–44.
35. Grigoryev,S.A., Arya,G., Correll,S., Woodcock,C.L. and Schlick,T. (2009) Evidence for heteromorphic chromatin fibers from analysis of nucleosome interactions. *Proc. Natl Acad. Sci. USA*, **106**, 13317–13322.
36. Gessner,R.V., Quigley,G.J., Wang,A.H., van der Marel,G.A., van Boom,J.H. and Rich,A. (1985) Structural basis for stabilization of Z-DNA by cobalt hexaammine and magnesium cations. *Biochemistry*, **24**, 237–240.
37. Ho,P.S., Frederick,C.A., Quigley,G.J., van der Marel,G.A., van Boom,J.H., Wang,A.H. and Rich,A. (1985) G•T wobble base-pairing in Z-DNA at 1.0 Å atomic resolution: the crystal structure of d(CGCGTG). *EMBO J.*, **4**, 3617–3623.
38. Cowan,J.A. (1995) *The Biological Chemistry of Magnesium*. VCH Publishers, New York.
39. Schalch,T., Duda,S., Sargent,D.F. and Richmond,T.J. (2005) X-ray structure of a tetranucleosome and its implications for the chromatin fibre. *Nature*, **436**, 138–141.
40. Sun,J., Zhang,Q. and Schlick,T. (2005) Electrostatic mechanism of nucleosomal array folding revealed by computer simulation. *Proc. Natl Acad. Sci. USA*, **102**, 8180–8185.
41. Wu,C., Bassett,A. and Travers,A. (2007) A variable topology for the 30-nm chromatin fibre. *EMBO Rep.*, **8**, 1129–1134.
42. Kepper,N., Foethke,D., Stehr,R., Wedemann,G. and Rippe,K. (2008) Nucleosome geometry and internucleosomal interactions control the chromatin fiber conformation. *Biophys. J.*, **95**, 3692–3705.
43. Kruithof,M., Chien,F.T., Routh,A., Logie,C., Rhodes,D. and van Noort,J. (2009) Single-molecule force spectroscopy reveals a highly compliant helical folding for the 30-nm chromatin fiber. *Nat. Struct. Mol. Biol.*, **16**, 534–540.
44. Falaschi,A. (2008) Similia similibus: pairing of homologous chromosomes driven by the physicochemical properties of DNA. *HFSP J.*, **2**, 257–261.
45. Duncan,I.W. (2002) Transvection effects in *Drosophila*. *Annu. Rev. Genet.*, **36**, 521–556.
46. Tsai,J.H. and McKee,B.D. (2011) Homologous pairing and the role of pairing centers in meiosis. *J. Cell Sci.*, **124**, 1955–1963.
47. Ding,D.Q., Okamasa,K., Yamane,M., Tsutsumi,C., Haraguchi,T., Yamamoto,M. and Hiraoka,Y. (2012) Meiosis-specific noncoding RNA mediates robust pairing of homologous chromosomes in meiosis. *Science*, **336**, 732–736.
48. Grimaud,C., Bantignies,F., Pal-Bhadra,M., Ghana,P., Bhadra,U. and Cavalli,G. (2006) RNAi components are required for nuclear clustering of Polycomb group response elements. *Cell*, **124**, 957–971.
49. Blumenstiel,J.P., Fu,R., Theurkauf,W.E. and Hawley,R.S. (2008) Components of the RNAi machinery that mediate long-distance chromosomal associations are dispensable for meiotic and early somatic homolog pairing in *Drosophila melanogaster*. *Genetics*, **180**, 1355–1365.
50. Bateman,J.R. and Wu,C.T. (2008) A genomewide survey argues that every zygotic gene product is dispensable for the initiation of somatic homolog pairing in *Drosophila*. *Genetics*, **180**, 1329–1342.
51. Cook,P.R. (1997) The transcriptional basis of chromosome pairing. *J. Cell Sci.*, **110**, 1033–1040.
52. McKee,B.D. (2004) Homologous pairing and chromosome dynamics in meiosis and mitosis. *Biochim. Biophys. Acta*, **1677**, 165–180.
53. Tang,S.J. (2011) Chromatin organization by repetitive elements (CORE): a genomic principle for the higher-order structure of chromosomes. *Genes*, **2**, 502–515.